

Bottomonium suppression: A probe to the pre-equilibrium era of quark matter

Uttam Kakade¹ Binoy Krishna Patra² and Lata Thakur³

Department of Physics, Indian Institute of Technology Roorkee, India, 247 667

Abstract

We have studied the thermal suppression of the bottomonium states in relativistic heavy-ion collision at LHC energies as function of centrality, rapidity, transverse momentum etc. to explain the CMS data. Our investigation mainly spans over three problems: a) how the theoretical predictions might still be modified by the remnants of the non-perturbative confining force, b) how does the presence of a not necessarily isotropic QCD medium modify the potential (both the real and imaginary part) acting between a static quark and antiquark pair, and c) finally how the additional time-zone of pre-equilibrium partonic evolution, in addition to the above modifications, affects the bottomonium production at the LHC energies. We resolve them by correcting both the perturbative and nonperturbative terms of the $Q\bar{Q}$ potential in (an)isotropic QCD medium and then couple to the dynamics of the system undergoing successive pre-equilibrium and equilibrium era. Due to the tiny formation time and the large binding energy of bottomonium (1S) state, we succeed in constraining the isotropization time and the shear viscosity.

PACS: 12.39.-x, 11.10.St, 12.38.Mh, 12.39.Pn 12.39.Hg; 12.38.Gc

1 Introduction

The experimental programs at Super Proton Synchrotron (SPS) at CERN, Relativistic Heavy Ion Collider (RHIC) at BNL and Large Hadron Collider (LHC) at CERN open up an window

¹usk11dph@iitr.ac.in

²binoyfph@iitr.ac.in

³lata1dph@iitr.ac.in

onto the properties of Quantum Chromodynamics (QCD) at high temperatures in guise of quark-gluon plasma (QGP). Following the conjecture of Matsui and Satz [1], there was considerable interest to study the properties of quarkonia at finite temperature. It was until recently that the inherent hierarchy of the scales in the heavy quark bound systems ($m_Q \gg m_Q v \gg m_Q v^2$) facilitates to derive a sequence of effective field theories (EFT) from the underlying theory, QCD, *namely* non relativistic QCD (NRQCD) and potential NRQCD (pNRQCD), by integrating out the successive scales in the system. The heavy quark bound states are described by the singlet and octet potentials through the matching coefficients in the effective lagrangian, which, however can be extended to finite temperature [2] with the additional thermal scales, T , gT , g^2T etc. The thermal corrections to the real and imaginary part of the singlet potential are manifested as the Debye screening [1] and the Landau damping [3, 4], respectively. On the other hand, the non EFT defines the potential from the late time behavior of a Wilson loop [2, 5, 6, 7, 8, 9, 10]. However, at finite temperature, the Wilson loop depends on imaginary time and the analytic continuation in the large real-time limit gives the (complex) potential [2, 10], whose imaginary part is manifested as Landau damping [3].

The separation of thermal scales in EFT is not evident and one needs lattice techniques to test the approach, where the dissociation of the quarkonium states can be studied even without the potential models rather the physics of a given quarkonium state is encoded in its spectral function in terms of the Euclidean meson correlation functions [11, 12, 13, 14, 15, 16]. However, the reconstruction of the spectral functions from the lattice meson correlators turns out to be very difficult. At finite temperature the situation becomes worse because the temporal extent is decreasing and particularly, for the bottomonium states, it becomes worst, thus inadvertently supports the use of potential models at finite temperature to complement the lattice studies.

The physical picture of quarkonium dissociation has been evolved over the years, where the properties of thermally produced heavy quarkonium states can be observed through the energy spectrum of their decay products [17, 18]. Thus the disappearance of the peak in the resonance peak hints the dissolution of the state. Physically a resonance is dissolved into a medium through the broadening of its width. In EFT framework, when the binding energy is large compared to the temperature, the resonances acquire a finite width due to interactions with ultra-soft gluons, causing the singlet-to-octet transitions [2]. This picture is relevant for the $\Upsilon(1S)$ suppression at the LHC. But when the binding energy is smaller than any of the above thermal scales, the potential acquires an imaginary component [2] (Landau Damping), which induces a thermal width. However

beyond the leading-order the above mentioned processes become entangled. On the other hand, in a non-EFT framework, the width arises either when a bound state absorbs a hard gluons or a light parton of the medium scatters off the bound state by exchanging a space-like gluon.

The (heavy) quark and antiquark ($Q\bar{Q}$) pairs are produced in heavy ion collisions on a very short time-scale ($\sim 1/2m_Q$), when the initial state effects on the parton densities (shadowing) [19], the initial state energy loss [20], the intrinsic heavy flavors, and the final state absorption on nucleons [19, 21] etc. could affect the production mechanism intimately. The shadowing and absorption are important at mid rapidity whereas the (initial-state) energy loss and intrinsic heavy flavor are important at forward rapidity. As the times are elapsed, the resonances are formed over a formation time, τ_F and traverses the plasma and then the hadronic matter before leaving the interacting system to be decayed into a dilepton. This long ‘trek’ inside the interacting system is cliffhanger for the pair. By the time the resonance is formed, either the screening of the color force [1] or an energetic gluon [22, 23], even a comoving hadron [24] could dissociate the resonance(s). Since the expansion of the matter produced in heavy-ion collisions proceeds through the successive stages of pre equilibrium (anisotropic) and equilibrium (isotropic) phases, therefore a study of quarkonium production is poised to provide a wealth of information about the evolution of the plasma and its in-medium properties.

In the early days of collider experiments at SPS and RHIC, most of the interests were focused on the suppression of $c\bar{c}$ bound states [1, 25] but several observations are yet to be understood *namely* the suppression of ψ (1S) does not increase from SPS to RHIC, even though the centre-of-mass energy is increased by fifteen times. The heavy-ion program at the LHC may resolve those puzzles because the beam energy and luminosity are increased by ten times of that of the RHIC. Moreover the CMS detector has excellent capabilities for muon detection and provides measurements of $\psi(2S)$ and the Υ family, which enables the quantitative analysis of quarkonia. That is why the interest may be shifted to the bottomonium states at the LHC energy due to the following reasons: i) The initial state effects to the bottomonium production are much smaller than the charmonium production. ii) The bottomonium is much heavier than the charmonium, the competition due to the recombination is thus unlikely. iii) Since the bottom quark is heavier, it can be dealt efficiently by the potential approach. iv) Although the Υ states have diverse binding energies but their similar decay kinematics and production mechanisms enable to measure their relative suppression unambiguously.

The works described above were limited to an isotropic medium but the system produced in relativistic heavy-ion collision may not be homogeneous and isotropic because at the early stages of the collision, the asymptotic weak-coupling enhances the longitudinal expansion substantially than the radial expansion. There have been significant advances in the dynamical models used to simulate plasma evolution with the momentum-space anisotropies in full (3+1)-dimensional simulations [26, 27, 28, 29]. In recent years, the effects of anisotropy on the quarkonia states have been extensively investigated [30, 31] by the leading-anisotropic correction to the perturbative term of the potential alone and found that the anisotropy can have a significant impact on quarkonium suppression. However, in the experimentally relevant regime of temperature (just above the crossover or transition temperature), the theoretical predictions based on high temperature methods, such as HTL perturbation theory might be modified by the remnants of the non-perturbative confining force [32]. Although the direct lattice QCD based determinations of the potential have progressed a lot, a model potential for the phenomenological descriptions of heavy quarkonium suppression would indeed be quite useful. This is one of the main goal of this present study and argue for the modification of the full Cornell potential as an appropriate potential for heavy quarkonium at finite temperature.

Recently we have investigated the properties of quarkonia states through the medium modifications to both the perturbative and nonperturbative terms of the $Q\bar{Q}$ potential [33] in the presence of a not necessarily isotropic QCD medium, which have mainly two important observations: The first one is that the inclusion of the confining string term, in addition to the Coulomb term makes both the real and imaginary parts of the potential more stronger, compared to the medium correction of the perturbative term of the potential alone [34]. Since the imaginary part contributes to the width (Γ) of quarkonium bound states [3, 4, 10] which in turn determines the dissociation temperatures, so the above cumulative effects due to the remnants of nonperturbative term dissociate the quarkonia states at higher temperatures. Secondly the presence of the anisotropy makes the real-part of the potential stronger but the imaginary-part becomes leaner and overall the anisotropy makes the quarkonia to dissociate at higher temperatures, compared to the isotropic medium. In the present work, we continue with our model potential [33] and numerically obtain the dissociation temperatures of the ground and the excited states of the Υ family (which was not done earlier in [33]). With these understandings about the quarkonia states in a static (an)isotropic medium, we move on to study the dynamical (sequential) suppression of the bottomonium states in nucleus-nucleus collisions at the LHC energies. We found that the

local equilibrium hydrodynamic regime alone may not be sufficient to suppress the bottomonium states adequately and some additional (pre-equilibrium) time zone of plasma evolution needs to be scanned, which seems plausible theoretically as well as experimentally. The unique features of the bottomonium (1S) state, *namely* the tiny formation time and large binding energy, facilitate to probe both the (pre-equilibrium) era prior to the isotropization time and the shear viscosity-to-the entropy ratio.

Our work is organized as follows. In Section 2, we revisited the anisotropic corrections to the retarded, advanced and symmetric gluon self energies and the corresponding (static) propagators in hard thermal loop perturbation theory [35] and then study the in-medium properties of the quarkonium states by the resulting complex potential (in Section 2.1 and 2.2, respectively). In Section 2.3, we study the dissociation through a complex potential by obtaining the real and imaginary part of the binding energies and calculate the dissociation temperatures of the ground and excited $b\bar{b}$ states. Next we switch over our discussion (in Section 3) to an expanding medium, which undergoes expansion through the successive pre-equilibrium and equilibrium era and study the survival of the bottomonium states by coupling the in-medium dissociation with the dynamics of the expansion. We found that our model explains the CMS data [36] reasonably well, apart from the uncertainties arising due to various initial-state effects, which is however expected to be very small for the bottomonium states at the LHC. Finally, we conclude in Section 4.

2 Bottomonium in anisotropic medium

An interesting property at the initial phase of the QGP is nowadays the anisotropies that occur [37, 38, 39]. It is therefore worthwhile to consider the properties of quarkonia such as the binding energy, decay width in such a system. The calculation of the real part of the potential at finite anisotropy was first obtained in Ref. [30, 38, 40] and was later extended for the imaginary part [2, 30, 41], by the leading anisotropic corrections to the perturbative term of the potential alone, which was further coupled with the dynamical evolution of the anisotropic plasma to quantify the quarkonium suppression in nuclear collisions [42, 43]. We now continue with the above works to derive the potential at finite temperature keeping both the perturbative and nonperturbative terms via the Keyldesh presentation in real-time formalism.

2.1 Real part of the potential

Since the mass of the heavy quark is very large, so both the requirements: $m_Q \gg \Lambda_{QCD}$ and $T \ll m_Q$ are met for the description of the interactions between a pair of heavy quark and antiquark at finite temperature, in terms of a quantum mechanical potential. We thus obtain the potential by correcting *both the short and long-distance part* of the $Q\bar{Q}$ potential, with a dielectric function, $\epsilon(p)$ [32] embodying the effect of the medium

$$V(r, T) = \int \frac{d^3\mathbf{P}}{(2\pi)^{3/2}} (e^{i\mathbf{P}\cdot\mathbf{r}} - 1) \frac{V(p)}{\epsilon(p)}. \quad (1)$$

We assume the same screening scales to regulate both terms (by multiplying with an exponential damping factor and is switched off after the Fourier transform is evaluated), to obtain the Fourier transform of the potential⁴:

$$V(p) = -\sqrt{(2/\pi)} \frac{\alpha}{p^2} - \frac{4\sigma}{\sqrt{2\pi}p^4}. \quad (2)$$

We will now obtain the dielectric permittivity through the leading anisotropic corrections to the self-energies and then to the static propagators in weak coupling HTL approximation. In Keldysh representation, the retarded (R), advanced (A) and symmetric (F) propagators can be written as the linear combination of the components of the (2×2) matrix propagator in real-time formalism:

$$D_R^0 = D_{11}^0 - D_{12}^0, \quad D_A^0 = D_{11}^0 - D_{21}^0, \quad D_F^0 = D_{11}^0 + D_{22}^0, \quad (3)$$

where only the symmetric component involves the distribution functions and is of particular advantage for the HTL diagrams where the terms containing distribution functions dominate. Similar relations hold good for the retarded (Π_R), advanced (Π_A) and symmetric (Π_F) self energies. Now the resummation of the propagators is done via the Dyson-Schwinger equation

$$D_{R,A} = D_{R,A}^0 + D_{R,A}^0 \Pi_{R,A} D_{R,A}, \quad (4)$$

$$D_F = D_F^0 + D_R^0 \Pi_R D_F + D_F^0 \Pi_A D_A + D_R^0 \Pi_F D_A. \quad (5)$$

For the static potential, we need only the temporal component (“00” \equiv L) of the propagator, whose evaluation is easier in the Coulomb gauge. Thus the above resummation (4) can be recast through its temporal component as

$$D_{R,A}^L(iso) = D_{R,A}^{L(0)} + D_{R,A}^{L(0)} \Pi_{R,A}^L(iso) D_{R,A}^L(iso). \quad (6)$$

⁴In Ref. [44, 45], different scales for the Coulomb and linear pieces were employed through a dimension-two gluon condensate.

The above relations are not satisfied for the anisotropic system due to the preferential direction of anisotropy. However, for anisotropic medium which exhibits a weak anisotropy ($\xi \ll 1$), we circumvent the problem, by expanding the propagators and self-energies in ξ :

$$D = D_{\text{iso}} + \xi D_{\text{aniso}}, \quad \Pi = \Pi_{\text{iso}} + \xi \Pi_{\text{aniso}}, \quad (7)$$

where the parameter ξ is a measure of the anisotropy

$$\xi = \frac{\langle \mathbf{p}_T^2 \rangle}{2\langle p_L^2 \rangle} - 1, \quad (8)$$

where $p_L = \mathbf{p} \cdot \mathbf{n}$ and $\mathbf{p}_T = \mathbf{p} - \mathbf{n}(\mathbf{p} \cdot \mathbf{n})$ are the components of momentum parallel and perpendicular to the direction of anisotropy, \mathbf{n} , respectively. Thus in the presence of small anisotropy, the (resummed) temporal component of the retarded (advanced) propagator becomes

$$D_{R,A}^L(\text{aniso}) = D_{R,A}^{L(0)} \Pi_{R,A}^L(\text{aniso}) D_{R,A}^L(\text{iso}) + D_{R,A}^{L(0)} \Pi_{R,A}^L(\text{iso}) D_{R,A}^L(\text{aniso}) \quad (9)$$

We will now calculate the temporal component of the retarded/advanced gluon self-energy in the HTL-approximation, where the leading isotropic contribution is

$$\Pi_{R,A}^L(\text{iso})(P) = m_D^2 \left(\frac{p_0}{2p} \ln \frac{p_0 + p \pm i\epsilon}{p_0 - p \pm i\epsilon} - 1 \right), \quad (10)$$

with the prescriptions $+i\epsilon$ ($-i\epsilon$), for the retarded and advanced self-energies, respectively and m_D^2 ($= \frac{g^2 T^2}{6}(N_f + 2N_c)$) is the square of Debye mass. The full anisotropic contribution is then

$$\Pi_{R,A}^L(\text{aniso})(P) = \frac{m_D^2}{6} (1 + 3 \cos 2\theta_p) + \Pi_{R(\text{iso})}^L(P) \left(\cos(2\theta_p) - \frac{p_0^2}{2p^2} (1 + 3 \cos 2\theta_p) \right), \quad (11)$$

Similarly the isotropic and anisotropic terms for the temporal component of the symmetric self-energy are given by

$$\begin{aligned} \Pi_{F(\text{iso})}^L(P) &= -2\pi i m_D^2 \frac{T}{p} \Theta(p^2 - p_0^2), \\ \Pi_{F(\text{aniso})}^L(P) &= \frac{3}{2} \pi i m_D^2 \frac{T}{p} \left(\sin^2 \theta_p + \frac{p_0^2}{p^2} (3 \cos^2 \theta_p - 1) \right) \Theta(p^2 - p_0^2). \end{aligned} \quad (12)$$

Thus the gluon self-energy is found to have both real and imaginary part which are responsible for the Debye screening and the Landau damping, respectively where the former is usually obtained from the retarded and advanced self energy and the later is obtained from the symmetric self energy alone.

Therefore the real part of the temporal component of retarded (or advanced) propagator in the static limit gives

$$\Re D_{R,A}^{00}(0,p) = -\frac{1}{(p^2 + m_D^2)} + \xi \frac{m_D^2}{6(p^2 + m_D^2)^2} (3 \cos 2\theta_p - 1), \quad (13)$$

and the static limit of the imaginary part of the temporal component of symmetric propagator is

$$\Im D_F^{00}(0,p) = \frac{-2\pi T m_D^2}{p(p^2 + m_D^2)^2} + \xi \left(\frac{3\pi T m_D^2}{2p(p^2 + m_D^2)^2} \sin^2 \theta_p - \frac{4\pi T m_D^4}{p(p^2 + m_D^2)^3} \left(\sin^2 \theta_p - \frac{1}{3} \right) \right) \quad (14)$$

We can now obtain the dielectric permittivity from the static limit of the “00”-component of gluon propagator

$$\epsilon^{-1}(p) = -\lim_{\omega \rightarrow 0} p^2 D_{11}^{00}(\omega, p), \quad (15)$$

where the real and imaginary parts of D_{11}^{00} can be written as

$$\Re D_{11}^{00}(\omega, p) = \frac{1}{2} (D_R^{00} + D_A^{00}) \quad \text{and} \quad \Im D_{11}^{00}(\omega, p) = \frac{1}{2} D_F^{00}. \quad (16)$$

The real-part of the potential is then obtained as

$$\begin{aligned} \Re V_{(aniso)}(\mathbf{r}, \xi, T) &= \int \frac{d^3 \mathbf{p}}{(2\pi)^{3/2}} (e^{i\mathbf{p}\cdot\mathbf{r}} - 1) \left(-\sqrt{(2/\pi)} \frac{\alpha}{p^2} - \frac{4\sigma}{\sqrt{2\pi} p^4} \right) \times \\ & p^2 \left[\frac{1}{(p^2 + m_D^2)} - \frac{\xi m_D^2}{6(p^2 + m_D^2)^2} (3 \cos(2\theta_p) - 1) \right] \\ &\equiv \Re V_{1(aniso)}(\mathbf{r}, \xi, T) + \Re V_{2(aniso)}(\mathbf{r}, \xi, T), \end{aligned} \quad (17)$$

where θ_p is the angle between \mathbf{r} and \mathbf{n} (direction of anisotropy) and $\Re V_{1(aniso)}(\mathbf{r}, \xi, T)$ and $\Re V_{2(aniso)}(\mathbf{r}, \xi, T)$ are the medium modifications corresponding to the Coulomb and string term, respectively, are given by ($\hat{r} = r m_D$)

$$\begin{aligned} \Re V_{1(aniso)}(r, \theta_r, T) &= -\alpha m_D \left[\left(\frac{e^{-\hat{r}}}{\hat{r}} + 1 \right) + \xi \left[\left(\frac{e^{-\hat{r}} - 1}{6} \right) \right. \right. \\ & \left. \left. + \left(\frac{e^{-\hat{r}}}{6} + \frac{e^{-\hat{r}}}{2\hat{r}} + \frac{e^{-\hat{r}}}{\hat{r}^2} + \frac{e^{-\hat{r}} - 1}{\hat{r}^3} \right) (1 - 3 \cos^2 \theta_r) \right] \right] \end{aligned} \quad (18)$$

and

$$\begin{aligned} \Re V_{2(aniso)}(r, \theta_r, T) &= \frac{2\sigma}{m_D} \left[\left(\frac{e^{-\hat{r}} - 1}{\hat{r}} + 1 \right) + 2\xi \left[\left(\frac{e^{-\hat{r}} - 1}{6\hat{r}} + \frac{e^{-\hat{r}} + 2}{12} \right) \right. \right. \\ & \left. \left. + \left(\frac{e^{-\hat{r}}}{\hat{r}^2} + \frac{5e^{-\hat{r}} + \hat{r}e^{-\hat{r}} + 1}{12\hat{r}} + \frac{e^{-\hat{r}} - 1}{\hat{r}^3} \right) (1 - 3 \cos^2 \theta_r) \right] \right] \end{aligned} \quad (19)$$

Thus the real-part of the potential in anisotropic medium becomes

$$\begin{aligned}
\Re V_{\text{aniso}}(r, \theta_r, T) &= \frac{2\sigma}{m_D} \left(\frac{e^{-\hat{r}} - 1}{\hat{r}} + 1 \right) - \alpha m_D \left(\frac{e^{-\hat{r}}}{\hat{r}} + 1 \right) + \xi \frac{e^{-\hat{r}}}{\hat{r}} \\
&\times \left[\frac{2\sigma}{m_D} \left(\frac{e^{\hat{r}} - 1}{\hat{r}^2} + \frac{\hat{r}^2 e^{\hat{r}} - 3}{3\hat{r}} - \frac{5e^{\hat{r}} - \hat{r} + 1}{12} \right) - \frac{\alpha m_D}{2} \left(\frac{e^{\hat{r}} - 1}{\hat{r}^2} - \frac{1}{\hat{r}} - \frac{2\hat{r}e^{\hat{r}} - \hat{r} + 3}{6} \right) \right. \\
&+ \left. \left[\frac{2\sigma}{m_D} \left(3\frac{e^{\hat{r}} - 1}{\hat{r}^2} - \frac{3}{\hat{r}} - \frac{e^{\hat{r}} + \hat{r} + 5}{4} \right) - \frac{\alpha m_D}{2} \left(3\frac{e^{\hat{r}} - 1}{\hat{r}^2} - \frac{3}{\hat{r}} - \frac{\hat{r} + 3}{2} \right) \right] \cos 2\theta_r \right] \\
&= \Re V_{\text{iso}}(r, T) + V_{\text{tensor}}(r, \theta_r, T). \tag{20}
\end{aligned}$$

Thus the anisotropy in the momentum space introduces an angular (θ_r) dependence, in addition to the inter particle separation (r), to the potential, in contrast to the r -dependence only in an isotropic medium. The potential becomes stronger with the increase of anisotropy because the (effective) Debye mass $m_D(\xi, T)$ in an anisotropic medium is always smaller than in an isotropic medium. In particular, the potential for quark pairs aligned in the direction of anisotropy are stronger than the pairs aligned in the transverse direction.

2.2 Imaginary part of the potential

The imaginary part of the potential is obtained by the medium corrections to both the non-perturbative part (string term) and perturbative part of the potential at $T=0$, by the imaginary part of the dielectric function (14):

$$\begin{aligned}
\Im V_{\text{(aniso)}}(\mathbf{r}, \xi, T) &= - \int \frac{d^3\mathbf{p}}{(2\pi)^{3/2}} (e^{i\mathbf{p}\cdot\mathbf{r}} - 1) \left(-\sqrt{\frac{2}{\pi}} \frac{\alpha}{p^2} - \frac{4\sigma}{\sqrt{2\pi}p^4} \right) p^2 \left[\frac{-\pi T m_D^2}{p(p^2 + m_D^2)^2} \right. \\
&+ \left. \xi \left[\frac{3\pi T m_D^2}{4p(p^2 + m_D^2)^2} \sin^2 \theta_p - \frac{2\pi T m_D^4}{p(p^2 + m_D^2)^3} \left(\sin^2 \theta_p - \frac{1}{3} \right) \right] \right] \\
&\equiv \Im V_{1(\text{aniso})}(\mathbf{r}, \xi, T) + \Im V_{2(\text{aniso})}(\mathbf{r}, \xi, T), \tag{21}
\end{aligned}$$

where $\Im V_{1(\text{aniso})}(\mathbf{r}, \xi, T)$ and $\Im V_{2(\text{aniso})}(\mathbf{r}, \xi, T)$ are the imaginary contributions corresponding to the Coulombic and linear terms in anisotropic medium, respectively: The contribution due to the perturbative term in the leading-order is given by [30]

$$\Im V_{1(\text{aniso})}(\mathbf{r}, \xi, T) = -\alpha T (\phi_0(\hat{r}) + \xi [\phi_1(\hat{r}, \theta_r) + \phi_2(\hat{r}, \theta_r)]), \tag{22}$$

where the functions $\phi_0(\hat{r})$, $\phi_1(\hat{r}, \theta_r)$ and $\phi_2(\hat{r}, \theta_r)$ are given by

$$\begin{aligned}\phi_0(\hat{r}) &= -\alpha T \left(-\frac{\hat{r}^2}{9} (-4 + 3\gamma_E + 3 \log \hat{r}) \right) \\ \phi_1(\hat{r}, \theta_r) &= \frac{\hat{r}^2}{600} [123 - 90\gamma_E - 90 \log \hat{r} + \cos 2\theta_r (-31 + 30\gamma_E + 30 \log \hat{r})] \\ \phi_2(\hat{r}, \theta_r) &= \frac{\hat{r}^2}{90} (-4 + 3 \cos 2\theta_r)\end{aligned}\quad (23)$$

Similarly the imaginary part due to the nonperturbative (linear) term has also the isotropic and anisotropic term:

$$\Im V_{2(aniso)}(r, \xi, T) = \frac{2\sigma T}{m_D^2} \left(\psi_0(\hat{r}) - \xi [\psi_1(\hat{r}, \theta_r) + \psi_2(\hat{r}, \theta_r)] \right), \quad (24)$$

where the functions $\psi_0(\hat{r})$, $\psi_1(\hat{r}, \theta_r)$ and $\psi_2(\hat{r}, \theta_r)$ are given by

$$\psi_0(\hat{r}) = \frac{\hat{r}^2}{6} + \left(\frac{-107 + 60\gamma_E + 60 \log(\hat{r})}{3600} \right) \hat{r}^4 + O(\hat{r}^5), \quad (25)$$

$$\psi_1(\hat{r}, \theta_r) = \int \frac{dz}{z(z^2 + 1)^2} \left[1 - \frac{3}{2} \left(\sin^2 \theta_r \frac{\sin z\hat{r}}{z\hat{r}} + (1 - 3 \cos^2 \theta_r) G(\hat{r}, z) \right) \right], \quad (26)$$

$$\psi_2(\hat{r}, \theta_r) = -\frac{4}{3} \int \frac{dz}{z(z^2 + 1)^3} \left[1 - 3 \left[\left(\frac{2}{3} - \cos^2 \theta_r \right) \frac{\sin z\hat{r}}{z\hat{r}} + (1 - 3 \cos^2 \theta_r) G(\hat{r}, z) \right] \right] \quad (27)$$

where

$$G(\hat{r}, z) = \frac{z\hat{r} \cos(z\hat{r}) - \sin(z\hat{r})}{(z\hat{r})^3} \quad (28)$$

Thus the imaginary part of the potential in anisotropic medium in the leading logarithmic order becomes

$$\begin{aligned}\Im V_{(aniso)}(r, \theta_r, T) &= -T \left(\frac{\alpha \hat{r}^2}{3} + \frac{\sigma \hat{r}^4}{30m_D^2} \right) \log\left(\frac{1}{\hat{r}}\right) \\ &+ \xi T \left[\left(\frac{\alpha \hat{r}^2}{5} + \frac{3\sigma \hat{r}^4}{140m_D^2} \right) - \cos^2 \theta_r \left(\frac{\alpha \hat{r}^2}{10} + \frac{\sigma \hat{r}^4}{70m_D^2} \right) \right] \log\left(\frac{1}{\hat{r}}\right)\end{aligned}\quad (29)$$

where the magnitude is found to be smaller than the isotropic medium and decreases with the anisotropy. In weak anisotropic limit, the imaginary part is a perturbation and thus provides an estimate for the (thermal) width for a particular resonance state:

$$\begin{aligned}\Gamma_{(aniso)} &= \int d^3\mathbf{r} |\Psi(r)|^2 \left[\alpha T \hat{r}^2 \log\left(\frac{1}{\hat{r}}\right) \left(\frac{1}{3} - \xi \frac{3 - \cos 2\theta_r}{20} \right) \right. \\ &\quad \left. + \frac{2\sigma T}{m_D^2} \hat{r}^4 \log\left(\frac{1}{\hat{r}}\right) \frac{1}{20} \left(\frac{1}{3} - \xi \frac{2 - \cos 2\theta_r}{14} \right) \right] \\ &= T \left(\frac{4}{\alpha m_Q^2} + \frac{12\sigma}{\alpha^2 m_Q^4} \right) \left(1 - \frac{\xi}{2} \right) m_D^2 \log \frac{\alpha m_Q}{2m_D},\end{aligned}\quad (30)$$

which shows that the in-medium thermal width in anisotropic medium becomes smaller than in isotropic medium and gets narrower with the increase of anisotropy. This is due to the fact that the width is proportional to the square of the Debye mass and the debye mass decreases with the anisotropy because the effective local parton density around a test (heavy) quark is smaller compared to isotropic medium.

2.3 Dissociation in a complex potential

In short-distance limit, the vacuum contribution dominates over the medium contribution even for the weakly anisotropic medium and for the long-distance limit, the potential (20) in high temperature approximation results a Coulomb plus a sub leading anisotropic contribution :

$$\Re V_{(\text{aniso})}(r, \theta_r, T) \stackrel{\hat{r} \gg 1}{\simeq} -\frac{2\sigma}{m_D^2 r} - \alpha m_D - \frac{5\xi}{12} \frac{2\sigma}{m_D^2 r} \left(1 + \frac{3}{5} \cos 2\theta_r\right) \quad (31)$$

$$\equiv \Re V_{\text{iso}}(\hat{r} \gg 1, T) + V_{\text{tensor}}(\hat{r} \gg 1, \theta_r, T), \quad (32)$$

where the anisotropic contribution ($V_{\text{tensor}}(\hat{r} \gg 1, \theta_r, T)$) is smaller than the isotropic one ($\Re V_{\text{iso}}(\hat{r} \gg 1, T)$), so the anisotropic part can be treated as perturbation. Therefore, the real part of binding energy may be obtained from the radial part of the Schrödinger equation (of the isotropic component) plus the first-order perturbation due to the anisotropic component as :

$$E_{\text{bin}}^{\text{aniso}} \stackrel{\hat{r} \gg 1}{\simeq} \left(\frac{m_Q \sigma^2}{m_D^4 n^2} + \alpha m_D \right) + \frac{2\xi}{3} \frac{m_Q \sigma^2}{m_D^4 n^2}, \quad (33)$$

In the intermediate-distance scale, the real part of the potential (20) does not look simple, the interaction becomes complex and needs to be solved numerically. Usually the time- dependent or independent Schrödinger equation is solved by the finite difference time domain method (FDTD) or matrix method, respectively. In the matrix method, the Schrödinger equation can be solved in a matrix form through a discrete basis, instead of the continuous real-space position basis spanned by the states $|\vec{x}\rangle$. Here the confining potential V is subdivided into N discrete wells with potentials V_1, V_2, \dots, V_{N+2} such that for i^{th} boundary potential, $V = V_i$ for $x_{i-1} < x < x_i$; $i = 2, 3, \dots, (N+1)$. Therefore for the existence of a bound state, there must be exponentially decaying wave function in the region $x > x_{N+1}$ as $x \rightarrow \infty$ and has the form:

$$\Psi_{N+2}(x) = P_E \exp[-\gamma_{N+2}(x - x_{N+1})] + Q_E \exp[\gamma_{N+2}(x - x_{N+1})], \quad (34)$$

where, $P_E = \frac{1}{2}(A_{N+2} - B_{N+2})$, $Q_E = \frac{1}{2}(A_{N+2} + B_{N+2})$ and, $\gamma_{N+2} = \sqrt{2\mu(V_{N+2} - E)}$. The eigenvalues can be obtained by identifying the zeros of Q_E . We have then obtained the real and

imaginary part of the binding energies of the bottomonium states (shown in Fig 1), which is found to increase with the anisotropy.

We now study the dissociation of the resonances when the binding energy decreases with the increase of the temperature and becomes equal to $\sim \Gamma$ [12, 46]. The dissociation temperatures (T_D 's) can also be obtained from the intersection of the binding energies obtained from the real and imaginary part of the potential [43, 47], respectively. The T_D 's for the Υ (1S) and Υ (2S) states are $1.97 T_c$ and $1.44T_c$, respectively (Table 1) in isotropic medium ($\xi = 0$) and increases with the increase of anisotropy ($\xi > 0$), *i.e.* the bottomonium states persist higher temperatures ($2.1 T_c$ for $\xi = 0.6$) in a anisotropic plasma, which can be parametrized as $T_{\text{aniso}}^D(\xi) \simeq T_{\text{iso}}^D (1 + \frac{\xi}{7})$, compared to the relation $T_{\text{aniso}}^D(\xi) = T_{\text{iso}}^D (1 + \frac{\xi}{6})$ by Laine et al.[31]. Our results are found relatively higher compared to similar calculation [43, 47], which may be due to the absence of three-dimensional medium modification of the linear term in their calculation.

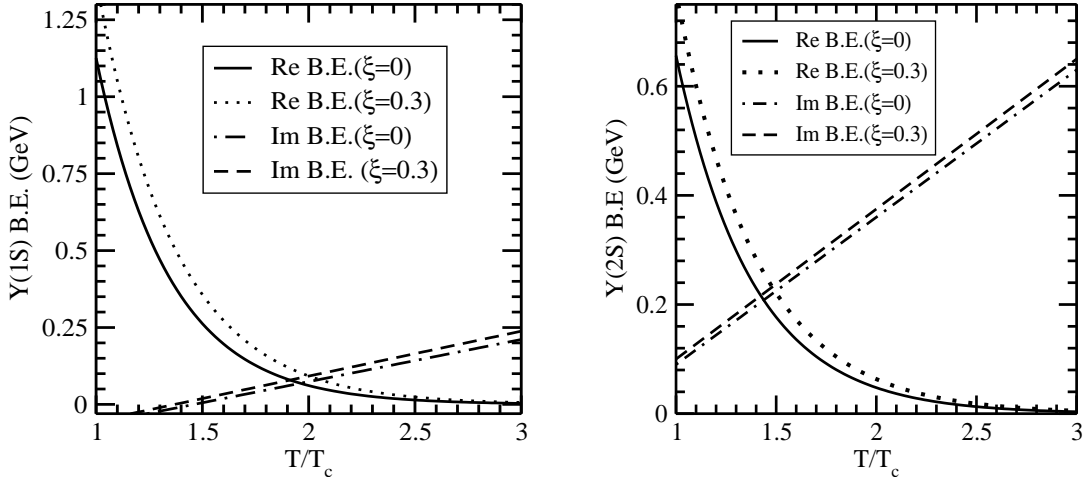


Figure 1: The real and imaginary part of the binding energies for the 1S and 2S states.

State	T_D			τ_F (fm)	ϵ_s ($\xi = 0$)	c_s^2
	$\xi = 0$	$\xi = 0.3$	$\xi = 0.6$			
$\Upsilon(1S)$	1.97	2.01	2.11	0.2	42.49	0.307
$\Upsilon(2S)$	1.44	1.50	1.54	0.4	12.74	0.284
$\Upsilon(3S)$	1.12	1.15	1.21	0.6	5.21	0.249
χ_{b1}	1.57	1.59	1.64	0.4	17.66	0.292

Table 1: Dissociation temperatures (T_D) in units of T_c for bottomonium states at different anisotropies (ξ) along with their (three sets) formation times (τ_F), screening energy densities (ϵ_s) and square of speed of sound (c_s^2) in isotropic medium.

3 Quarkonium in expanding medium

Let us now consider a nucleus-nucleus collision, where the partons are formed at time $\tau_i \sim Q_s^{-1}$ (Q_s is the saturation scale) and the system started evolving. There may be three plausible scenarios in space-time evolution *viz.* i) the partons are initially isotropized ($\tau_i = \tau_{iso}$), i.e., the system evolves hydrodynamically, ii) the system never isotropizes ($\tau_{iso} \rightarrow \infty$), i.e., it undergoes free streaming motion and iii) finally the system takes finite time to isotropize ($\tau_i < \tau < \tau_{iso}$), i.e., undergoes through successive anisotropic (pre-equilibrium) and isotropic (equilibrium) phases. The pre-equilibrium era may be conceived by the fact that the asymptotic weak-coupling at the early stage of the collision enhances the expansion in the beam direction (longitudinal) substantially than the radial expansion and results an anisotropy. This anisotropy makes the partonic system unstable with respect to the chromo magnetic plasma modes [48], which facilitate the system to isotropize quickly [37, 49, 50]. Recently there have been significant advances in the dynamical models for the plasma evolution to incorporate the momentum anisotropy [51, 52, 53].

Let us consider a region of energy density in the transverse plane, which is greater than or equal to the screening energy density, ϵ_s ($\propto T_D^4$). During the expansion, if the system has been cooled to an energy density less than or equal to ϵ_s , the $Q\bar{Q}$ pair would escape and form the (quarkonium) resonance. On the other hand if the energy density is still higher than ϵ_s , the resonance will not form and suppress the quarkonium production. Thus the pattern of suppression of the quarkonium states depends on how rapidly the system cools and how large is the screening energy density of the particular resonance state. The former depends on how to model the evolution of the system, where the equation of state needed to close the hydrodynamic equations is still not clear and how to incorporate the dissipative forces in the dynamics. The later (the screening energy density) depends on the properties of quarkonium states in the medium (which may or may not

be isotropic). However, the (finite) formation time and the intrinsic transverse momentum of the resonance enrich the suppression pattern more interesting.

Thus the discussion on the suppression of resonances in expanding medium is three fold respects: First we discuss on the equation of state (EOS) which gives the speed of sound (which controls the expansion of the medium) as a function of temperature, in contrast to the constant value usually adopted in the literature and use the EOS to evaluate the screening energy density corresponding to the temperature T_D . Secondly we discuss the evolution of the system first through the pre-equilibrium era and subsequently the (local) equilibrium era in the Bjorken boost-invariant expansion in the presence of dissipative forces in the stress tensor. Finally the above ingredients are coupled to quantify the suppression of the bottomonium states at the LHC.

3.1 Lattice equation of state

The pressure is the primary observable to study the QCD equation of state which, at finite chemical potential (μ_i), can be written through the Taylor-expansion [54]:

$$\frac{p(T, \{\mu_i\})}{T^4} = \frac{p(T, \{0\})}{T^4} + \frac{1}{2} \sum_{i,j} \frac{\mu_i \mu_j}{T^2} \chi_2^{ij}, \quad (35)$$

with the susceptibilities

$$\chi_2^{ij} \equiv \left. \frac{T}{V} \frac{1}{T^2} \frac{\partial^2 \log \mathcal{Z}}{\partial \mu_i \partial \mu_j} \right|_{\mu_i = \mu_j = 0}. \quad (36)$$

The trace anomaly, $I(T, \mu)$ is another quantity of interest in equation of state which can be obtained from the relation:

$$\frac{I(T, \mu)}{T^4} \equiv \frac{\epsilon(T, \mu) - 3p(T, \mu)}{T^4} = \frac{I(T, 0)}{T^4} + \frac{\mu^2}{2T} \frac{\partial \chi_2}{\partial T} \quad (37)$$

In the limit of vanishing baryon chemical potential, the trace anomaly and the Taylor-coefficients (susceptibilities) was parametrized [54] as

$$\frac{I(T)}{T^4} = e^{-h_1/t - h_2/t^2} \left[h_0 + \frac{f_0 [\tanh(f_1 t + f_2) + 1]}{1 + g_1 t + g_2 t^2} \right]. \quad (38)$$

$$\chi_2(T) = e^{-h_3/t - h_4/t^2} f_3 [\tanh(f_4 t + f_5) + 1], \quad (39)$$

where $t = T/200$ and the values of other parameters are given in [54].

The inverse relation between the pressure and the trace anomaly at $\mu = 0$ then becomes

$$\frac{p(T, 0)}{T^4} = \int_0^T dT' \frac{I(T', 0)}{T'^5}. \quad (40)$$

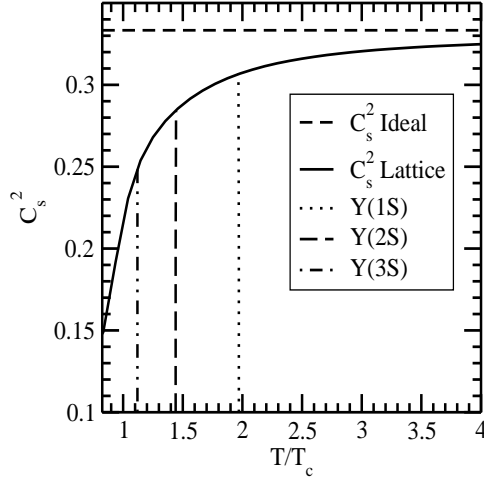


Figure 2: variation of the speed of sound

The energy density ϵ is then obtained from the trace anomaly and the pressure

$$\epsilon = I + 3p , \quad (41)$$

hence the speed of sound c_s can be obtained from the relation:

$$c_s^2 = \left. \frac{\partial p}{\partial \epsilon} \right|_{s/n} . \quad (42)$$

We have shown that how the speed of sound varies with temperature rapidly in the vicinity of the critical point and approaches towards the asymptotically ideal value (1/3) (in Fig.2) for very high temperature. In particular we have marked the values of c_s^2 's at the dissociation temperatures (T_D 's) of the Υ (nS) states and indicates that how the expansion of the system deviates from the ideal one at T_D 's and hence has a large bearing on the suppression.

Thus the equation of state can be used to calculate the energy density (ϵ_s) at the dissociation temperature (T_D) and also be used as an input to the hydrodynamics equation of motion. Another important quantity in the quarkonium suppression is the screening time, which can also be obtained from the screening energy density ϵ_s and the speed of sound.

3.2 Evolution in pre-equilibrium era

The evolution of the pre-equilibrium (anisotropic) hydrodynamics may be dealt in two ways: the first one is a phenomenological and refers directly to tensor structure of an anisotropic fluid [27,

28, 29] and the second one employs the transport equation for the gluon distribution function in the anisotropic background [26]. Phenomenologically the generalized anisotropy parameter can be written in (1+1) dimension

$$\xi(\tau, \delta) = \left(\frac{\tau}{\tau_i} \right)^\delta - 1, \quad (43)$$

where the interpolating co-efficient, δ characterizes the various isotropization process, *viz.* the asymptotic limits $\delta \rightarrow 0$ and 2 represent the (local equilibrium) hydrodynamics and the free-streaming, respectively whereas the intermediate values $1/6 \leq \delta \leq 1/2$ and $2/3$ denote the plasma instability and the collisional broadening, respectively. For the general value of δ , the proper time dependence of the energy density, the hard momentum scale and the number density for large times, $\tau \gg \tau_i$, can be written as,

$$\varepsilon(\tau) = \varepsilon_0 \left(\frac{\tau_i}{\tau} \right)^{4(1-\delta/8)/3}, \quad (44)$$

$$p_{\text{hard}}(\tau) = T_0 \left(\frac{\tau_i}{\tau} \right)^{(1-\delta/2)/3}, \quad (45)$$

$$n(\tau) = n_0 \left(\frac{\tau_i}{\tau} \right), \quad (46)$$

respectively. The smoothness of the transition from a non zero value (of δ) to 0 at $\tau \sim \tau_{\text{iso}}$, is governed by a smeared step function $\lambda(\tau)$ [26, 53],

$$\lambda(\tau) = \frac{1}{2} \left[\tanh\left(\frac{\gamma(\tau - \tau_{\text{iso}})}{\tau_i} \right) + 1 \right], \quad (47)$$

where the parameter, γ sets the sharpness of the transition from pre-equilibrium to (local equilibrium) hydrodynamic behavior. Thus the above dependence, in terms of $\lambda(\tau)$, become

$$\xi(\tau, \delta) = \left(\frac{\tau}{\tau_i} \right)^{\delta(1-\lambda(\tau))} - 1 \quad (48)$$

$$\mathcal{E}(\tau) = \mathcal{E}_0 \mathcal{R}(\xi) \bar{\mathcal{U}}^{4/3} \quad (49)$$

$$p_{\text{hard}}(\tau) = T_0 \bar{\mathcal{U}}^{1/3} \quad (50)$$

where the functions $\mathcal{R}(\xi)$ and $\bar{\mathcal{U}}$ are given by

$$\mathcal{R}(\xi) = \frac{1}{2} \left(\frac{1}{\xi + 1} + \frac{\tan^{-1} \sqrt{\xi}}{\sqrt{\xi}} \right), \quad (51)$$

$$\bar{\mathcal{U}} = \mathcal{U}(\tau)/\mathcal{U}(\tau_i), \quad (52)$$

with

$$\mathcal{U}(\tau) \equiv \left[\mathcal{R} \left(\left(\frac{\tau_{\text{iso}}}{\tau_i} \right)^\delta - 1 \right) \right]^{3\lambda(\tau)/4} (\tau_{\text{iso}}/\tau)^{1-\delta(1-\lambda(\tau))/2}. \quad (53)$$

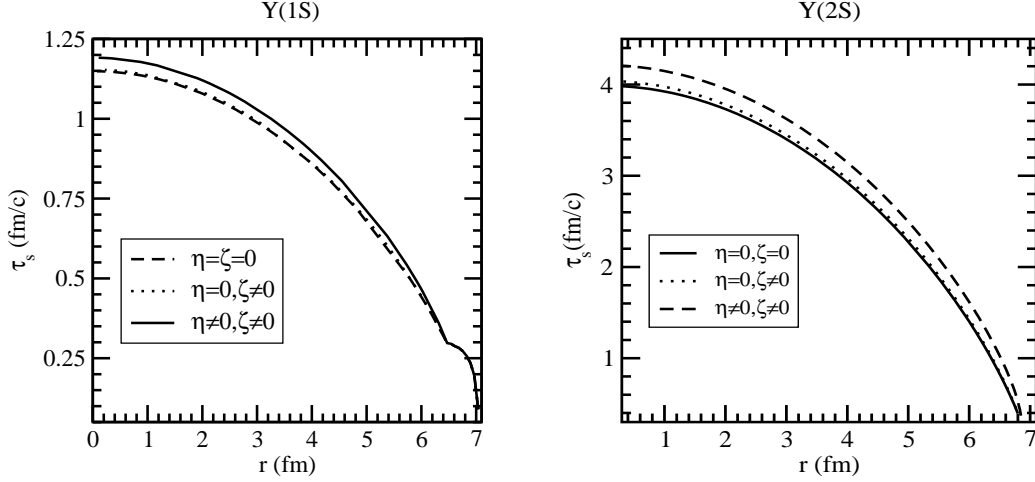


Figure 3: Constant energy density contour for the Υ (1S) (left panel) and the Υ (2S) (right panel) for different values of shear (η) and bulk (ζ) viscosities.

3.3 Evolution in equilibrium era: Bjorken expansion

When the rate of interaction overcomes the expansion rate the system attains local thermodynamic equilibrium for times $\tau \geq \tau_{iso}$. The energy momentum tensor of the plasma in the absence of dissipative forces is written as:

$$T^{\mu\nu} = (\epsilon + p)u^\mu u^\nu + g^{\mu\nu}p, \quad (54)$$

where ϵ and p are the energy density and the pressure, respectively. Then the Bjorken's boost-invariant longitudinal expansion gives the equation of motion:

$$\frac{d\epsilon}{d\tau} = -\frac{\epsilon + p}{\tau}, \quad (55)$$

where the equation of state ($p = c_s^2 \epsilon$) has been coupled to give rise

$$\epsilon(\tau)\tau^{1+c_s^2} = \epsilon(\tau_i)\tau_i^{1+c_s^2}. \quad (56)$$

Now we study the corrections to the Bjorken expansion due to the dissipative forces in the energy-momentum tensor:

$$T^{\mu\nu} = (\epsilon + p)u^\mu u^\nu + g^{\mu\nu}p + \Pi^{\mu\nu}, \quad (57)$$

where the dissipative part (viscous stress tensor), $\Pi^{\mu\nu}$ is given by

$$\Pi^{\mu\nu} = \eta \left(\nabla^\mu u^\nu + \nabla^\nu u^\mu - \frac{2}{3} \nabla^{\mu\nu} \nabla^\rho u_\rho \right) + \zeta \nabla^{\mu\nu} \nabla^\rho u_\rho, \quad (58)$$

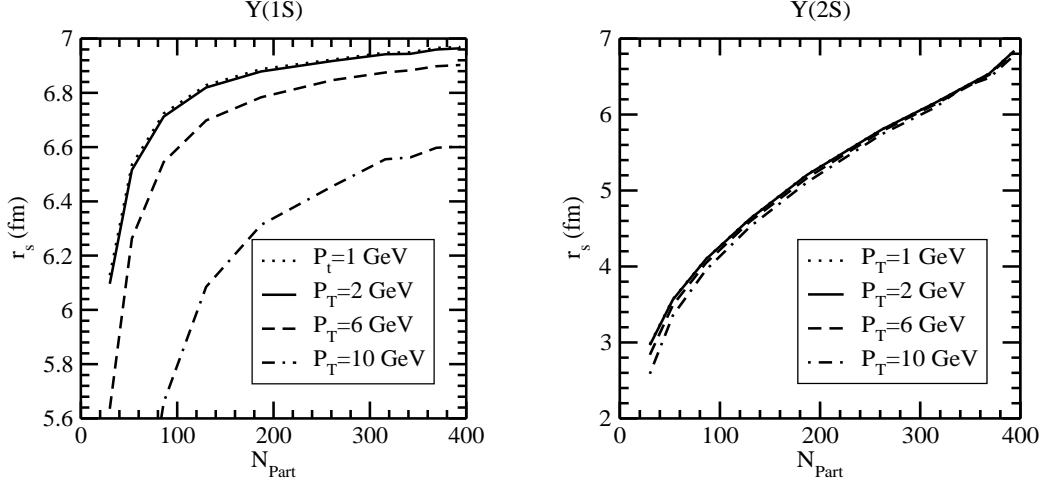


Figure 4: Centrality dependence of screening radius at fixed P_T for $\Upsilon(1S)$ (Left panel) and $\Upsilon(2S)$ (right panel).

where η and ζ are the shear and bulk viscosities, respectively and $\nabla^\mu = \nabla^{\mu\nu}\partial_\nu$ with $\nabla^{\mu\nu} = g^{\mu\nu} - u^\mu u^\nu$. In first-order viscous hydrodynamics, the bulk and shear stresses can be written in a gradient expansion:

$$\Pi = -\zeta\partial^\mu u_\mu, \quad \pi^{\mu\nu} = \eta\langle\nabla^\mu u^\nu\rangle, \quad (59)$$

where $\langle\nabla^\mu u^\nu\rangle$ is the symmetrized velocity gradient. The Israel-Stewart theory of second-order dissipative hydrodynamics [55] modifies the equation of motion for the ideal fluid (57) into [56, 57, 58, 59]

$$\frac{d\epsilon}{d\tau} = -\frac{1}{\tau}(\epsilon + p - \Phi + \Pi), \quad (60)$$

where the bulk (Π) and the shear stress (Φ) will asymptotically (after the relaxation times τ_Π and τ_π , respectively) reduce to their first-order values. In the Navier-Stokes limit, the one-dimensional boost-invariant expansion gives [60],

$$\Phi = \frac{4\eta}{3\tau}, \quad \Pi = -\frac{\zeta}{\tau}. \quad (61)$$

Substituting the values of Φ and Π in (60), the Bjorken longitudinal expansion can be read as:

$$\frac{d\epsilon}{d\tau} + \frac{\epsilon + p}{\tau} = \frac{4\eta}{3} + \frac{\zeta}{\tau^2}, \quad (62)$$

whose solution can be obtained with the EoS $p = c_s^2\epsilon$,

$$\epsilon(\tau)\tau^{1+c_s^2} + c \left[\frac{4\eta}{3s} + \frac{\zeta}{s} \right] \frac{\tau^{1+c_s^2}}{\tilde{\tau}^2} = \epsilon(\tau_i)\tau_i^{1+c_s^2} + c \left[\frac{4\eta}{3s} + \frac{\zeta}{s} \right] \frac{\tau_i^{1+c_s^2}}{\tilde{\tau}_i^2} \quad (63)$$

where the constant, c is $(1 + c_s^2)a_f T_i^3 \tau_i$ with $a_f = (16 + 21n_f/2)\pi^2/90$, and $\tilde{\tau}^2$ (or $\tilde{\tau}_i^2$) are denoted by $(1 - c_s^2)\tau^2$ ($(1 - c_s^2)\tau_i^2$), respectively. The first term in both LHS and RHS accounts for the contributions coming from the zeroth-order expansion while the second term is due to the viscous corrections.

In the present work we use the shear viscosity to-entropy ratio, η/s from the perturbative QCD [61] and AdS/CFT calculations [62], whereas for the bulk-viscosity, ζ/s we consider the parametrization in [63, 64, 65], which suggest a sharp peak in the vicinity of T_c and is tiny below T_c [66]:

$$\zeta/s = \begin{cases} a_1 \exp\left(\frac{T-T_c}{\Delta T}\right) + b_1 \left(\frac{T}{T_c}\right)^2 & \text{if } T > T_c \\ a_1 \exp\left(\frac{10(T_c-T)}{\Delta T}\right) + \frac{b_1}{10} \left(\frac{T}{T_c}\right)^2 & \text{if } T_c \geq T \end{cases}, \quad (64)$$

where the parameter a_1 ($=0.901$) and the ΔT ($=T_c/14.5$) controls the height and the width of the curve, both of which are not well understood and may be varied considerably. The parameter b_1 ($=0.061$) is obtained by fitting Meyers central value of ζ/s at higher temperatures [63].

3.4 Survival of $b\bar{b}$ states

Let us take a simple parametrization for the initial energy density profile on the transverse plane:

$$\epsilon(\tau_i, r) = \epsilon_i A_T(r), \quad (65)$$

with the profile function

$$A_T(r) = \left(1 - \frac{r^2}{R_T^2}\right)^\beta \theta(R_T - r) \quad (66)$$

where r is the transverse co-ordinate, R_T is the transverse radius of the nucleus, and β represents the proportionality of the deposited energy to the nuclear thickness. Thus the average initial energy density, $\langle\epsilon_i\rangle$ can be obtained as

$$\epsilon_i = (1 + \beta)\langle\epsilon_i\rangle, \quad (67)$$

With this initial energy density profile (65), we now obtain the screening time ($\tau_s(r)$), when the energy density drops to the screening energy density ϵ_s , and construct the screening energy density contour. Since the system evolves through the successive pre-equilibrium and equilibrium era, so the entire contour is obtained by amalgamating the contours in pre-equilibrium and the equilibrium era. The contour in the pre-equilibrium era is obtained from the energy density (49)

whereas the equilibrium era gives the contour:

$$\tau_s(r) = \tau_i \left(\frac{\tilde{\tau}_s}{\tilde{\tau}_i} \right)^{2/1+c_s^2} \left[\frac{\epsilon_i(r) \tilde{\tau}_i^2 + c \left(\frac{4\eta}{3s} + \frac{\zeta}{s} \right)}{\epsilon_s \tilde{\tau}_s^2 + c \left(\frac{4\eta}{3s} + \frac{\zeta}{s} \right)} \right]^{1/1+c_s^2}, \quad (68)$$

The significance of the contour can be understood as follows: If a $Q\bar{Q}$ pair is produced inside the contour, the pair cannot escape and hence the resonance cannot be formed. If it is produced outside the contour, it survives. Since the $Q\bar{Q}$ pair takes finite time (τ_F) to form the physical resonances (J/ψ , Υ etc.), the boundary of the region (r_s), where the quarkonium formation is suppressed, has been quantified by equating the duration of screening time $\tau_s(r)$ to the formation time t_F in the plasma frame ($=\gamma\tau_F$, where γ is the dilation factor). For the equilibrium era undergoing through the Bjorken boost-invariant expansion, the screening radius can be calculated as:

$$r_s = R_T(1-A)^{\frac{1}{2}} \Theta(1-A), \quad (69)$$

$$A = \left[\frac{\epsilon_s}{\epsilon_i} \left(\frac{t_F}{\tau_i} \right)^{1+c_s^2} + \frac{c \left(\frac{4\eta}{3s} + \frac{\zeta}{s} \right)}{\epsilon_i} \left(\frac{(t_F/\tau_i)^{1+c_s^2}}{\tilde{\tau}_s^2} - \frac{1}{\tilde{\tau}_i^2} \right) \right]^{1/\beta}, \quad (70)$$

which depends on the initial conditions, the dynamics of the evolution, and also the dynamical properties of the resonance states. Since the initial conditions are related to the centrality of the collisions, thus the screening boundary gives rise to a centrality dependent suppression pattern. Suppose a $Q\bar{Q}$ pair is created initially at \mathbf{r}_0 with the transverse momentum \mathbf{p}_T on the transverse plane. By the time the resonance is formed, the pair moves then to a new position $\mathbf{r} = \mathbf{r}_0 + t_F \mathbf{p}_T / M$ and if $|\mathbf{r}|$ is greater than or equal to the screening radius r_s , the pair will escape the deadly contour, otherwise the resonance will never be formed. This gives rise to a characteristic dependence of p_T in the suppression pattern as well as the inequalities of the cosine of the angle between \mathbf{r} and \mathbf{p}_T vectors:

$$\cos \phi \geq [(r_s^2 - r^2) M - \tau_F^2 p_T^2 / M] / [2 r \tau_F p_T], \quad (71)$$

which leads to a range of values of ϕ when the quarkonium would escape.

Now we can write for the survival probability of the quarkonium:

$$S(p_T) = \left[\int_0^{R_T} r dr \int_{-\phi_{\max}}^{+\phi_{\max}} d\phi P(\mathbf{r}, \mathbf{p}_T) \right] / \left[2\pi \int_0^{R_T} r dr P(\mathbf{r}, \mathbf{p}_T) \right], \quad (72)$$

where ϕ_{\max} is the maximum positive angle ($0 \leq \phi \leq \pi$) allowed by Eq.(71):

$$\phi_{\max} = \begin{cases} \pi & \text{if } y \leq -1 \\ \cos^{-1} |y| & \text{if } -1 < y < 1 \\ 0 & \text{if } y \geq 1 \end{cases}, \quad (73)$$

with

$$y = [(r_s^2 - r^2) M - \tau_F^2 p_T^2 / M] / [2 r \tau_F p_T], \quad (74)$$

M is the mass of the resonance and P is the probability for the quark-pair production at $(\mathbf{r}, \mathbf{p}_T)$, in a hard collision which may be factored out as

$$P(\mathbf{r}, \mathbf{p}_T) = f(r)g(p_T), \quad (75)$$

where we take the profile function $f(\mathbf{r})$ as

$$f(r) \propto \left[1 - \frac{r^2}{R_T^2}\right]^\alpha \theta(R_T - r). \quad (76)$$

Often experimental measurement of survival probability at a given number of participants (N_{part}) or rapidity (y) is reported in terms of the p_T -integrated yield ratio:

$$\langle S \rangle = \frac{\int_{p_T^{\min}}^{p_T^{\max}} dp_T S(p_T)}{\int_{p_T^{\min}}^{p_T^{\max}} dp_T}. \quad (77)$$

The production of $b\bar{b}$ mesons occur in-part through the production of higher excited $b\bar{b}$ states and their decay into the ground state. Since the ground and excited states have different sizes (binding energies), the excited states will dissolve earlier compared to the tightly bound ground states, so a sequential suppression results. However, the situation may not be that simple because the states have different formation times too, opposite to their binding energies. So while calculating the p_T -integrated inclusive survival probability for individual states, the feed-down corrections may be taken into account as:

$$\langle S \rangle^{\text{incl}}(3S) = \langle S \rangle(3S), \quad (78)$$

$$\langle S \rangle^{\text{incl}}(2S) = f_1 \langle S \rangle(2S) + f_2 \langle S \rangle(3S), \quad (79)$$

$$\langle S \rangle^{\text{incl}}(1S) = g_1 \langle S \rangle(1S) + g_2 \langle S \rangle \chi_{b1} + g_3 \langle S \rangle(2S) + g_4 \langle S \rangle(3S), \quad (80)$$

where the branching factors f_i 's and g_i 's are obtained from the CDF measurement [67], where g_i 's are 0.509, 0.271, 0.107 and 0.113, respectively, assuming the survival probabilities of $\Upsilon(3S)$ and $\chi_b(2P)$ are same with g_4 as combined fraction while factors f_1 and f_2 are taken as 0.5. To study the centrality dependence of the suppression factor, we use the CMS measurements of the pseudo rapidity and centrality dependent transverse energy density in Pb-Pb collisions at the LHC energy [68], to obtain the initial condition:

$$\langle \epsilon_i \rangle = \frac{\xi}{A_T c \tau_i} J(y, \eta) \frac{dE_T}{d\eta}, \quad (81)$$

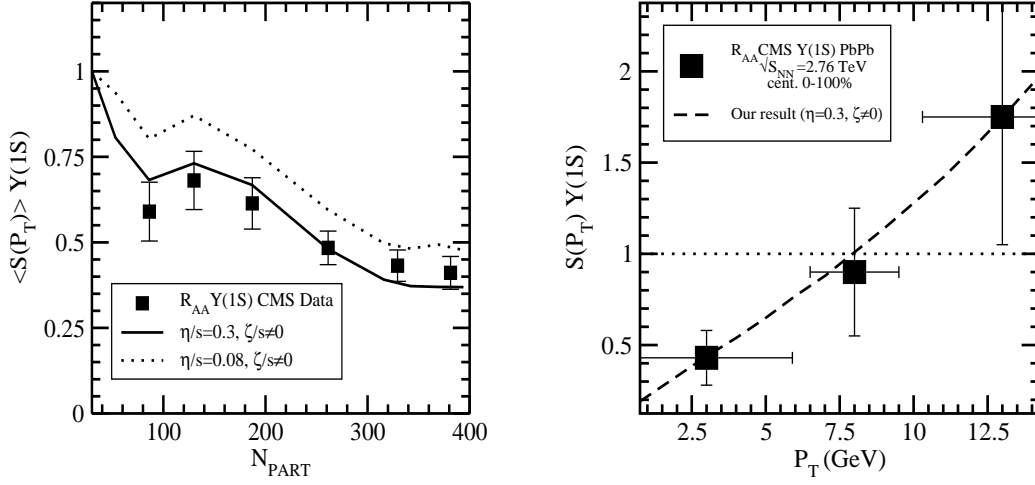


Figure 5: Centrality dependence of suppression factor for $\Upsilon(1S)$ (left panel) and variation of suppression factor against P_T for $\Upsilon(1S)$ (right panel).

where the Jacobian $J(y, \eta)$ ($=1.09$) is taken from HYDJET 1.8 for the pseudorapidity range $|\eta| < 0.35$ in central collisions at $\sqrt{s_{NN}} = 2.76$ TeV [69].

For the top 5% central (Pb-Pb) collisions at the LHC, the Bjorken formula (81) (without the factor, ξ) estimates the (initial) energy density, $\langle \epsilon \rangle_i = 14$ GeV/ $f m^3$ for initial time $\tau_i = 1$ fm. Although this estimate is 2.6 times larger than that at RHIC energy [68], but it underestimates the initial energy density to the extent such that even the excited states of Υ family have not been dissolved by the deconfined medium. So a scale factor ($\xi \sim 5$) has been introduced in the Bjorken formula to get rid of the unusually smaller values [70].

3.5 Results and discussions

Quarkonium suppression in nucleus-nucleus collisions compared to $p-p$ collisions involves various time-scales, associated with a) the initial conditions of the medium, b) the dynamics of the expansion, and the in-medium properties of the quarkonium states and finally the competition among them ensues a rich structure in the suppression pattern. The first one is related to the time scale of thermalization, the second one is associated to the formation of resonances in the dilated (fireball) frame (t_F), which depend on their intrinsic transverse momenta and the formation times in their rest frame, and are related through a hierarchy: $\tau_F(1S) < \tau_F(2S) < \tau_F(3S)$. The second is related to the expansion rate of the medium that can be effectively gauged in terms of the speed of sound,

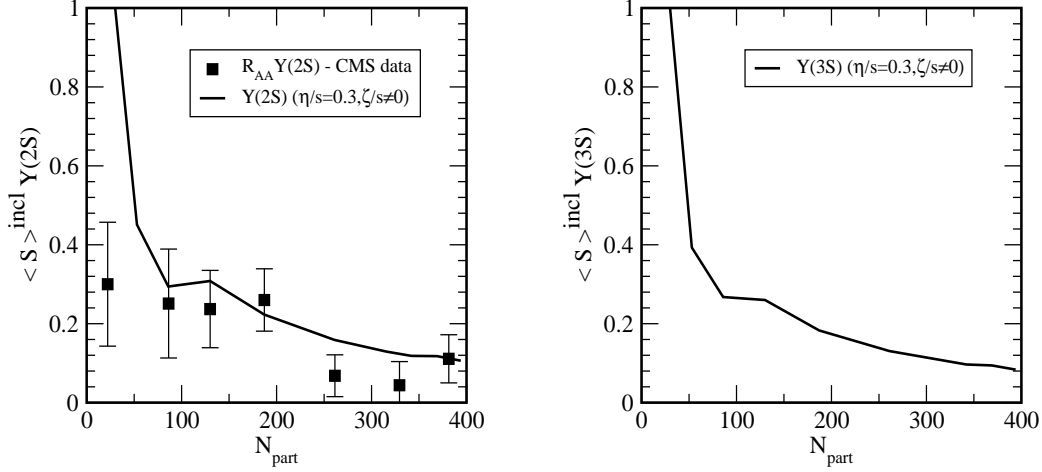


Figure 6: The centrality dependence of the inclusive survival probability of the 2S(left panel) and 3S(right panel) states, respectively.

which, in turn, is interconnected through the equation of state ($p = c_s^2 \epsilon$). The third one is the screening time, τ_s (the time-span of the suppression) which depends on the scale of dissociation (the screening energy, ϵ_s) and the speed of sound, c_s . The time τ_s also depends on the centrality of the collision (initial conditions), i.e., if the collision is more central then the system starts initially from the higher energy density and take longer time to reach ϵ_s . On the other hand, since the excited states are dissociated at lower temperatures compared to the ground state, so ϵ_s 's satisfy the hierarchy: $\epsilon_s(1S) \gg \epsilon_s(2S) \gg \epsilon_s(3S)$, hence the screening times, τ_s 's will thus satisfy the reverse relation: $\tau_s(1S) < \tau_s(2S) < \tau_s(3S)$. However, the hierarchy in the screening times, in conjunction with the formation times makes the suppression pattern complicated, *for example* the suppression of $\Upsilon(2S)$ state may not always larger than $\Upsilon(1S)$ state and the $\Upsilon(3S)$ state may not be suppressed more than the $\Upsilon(2S)$ state.

We will now discuss how the competition of the various time-scales transpires into the suppression pattern. Suppose if $\epsilon_s \gtrsim \epsilon_i$, there will be no suppression and if $\epsilon_i \gtrsim \epsilon_s$, there will be suppression but the extent of suppression depends on i) how big the difference, Δ ($=\epsilon_i - \epsilon_s$) is

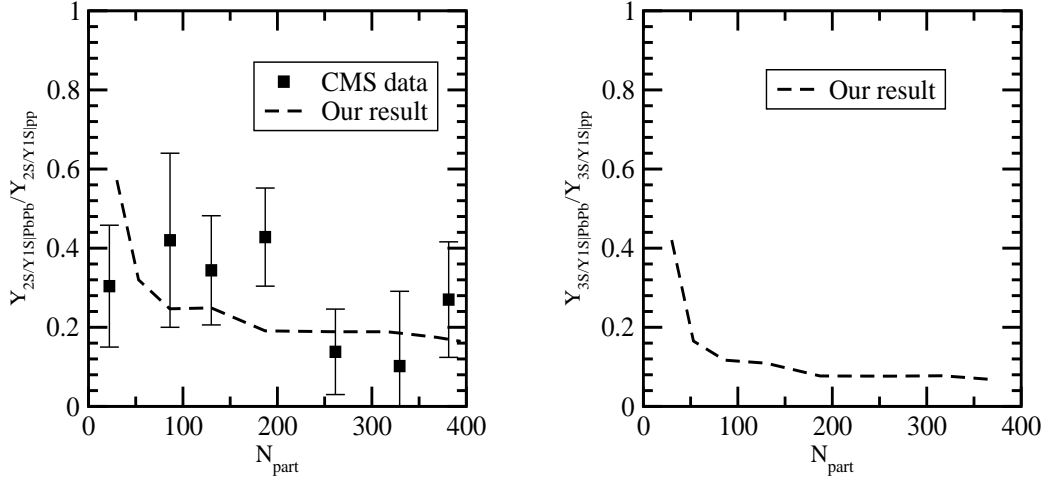


Figure 7: Centrality dependence of the double ratio $\frac{\Upsilon(2S)/\Upsilon(1S)|PbPb}{\Upsilon(2S)/\Upsilon(1S)|pp}$ (left panel) and $\frac{\Upsilon(3S)/\Upsilon(1S)|PbPb}{\Upsilon(3S)/\Upsilon(1S)|pp}$ (right panel) respectively.

between ϵ_i and ϵ_s and it varies from one state to other, and ii) how fast the system reaches to different ϵ_s 's, i.e., how large the screening time, τ_s is for different states, which in turn can be modulated by the bulk and shear forces near and away from the critical temperature, respectively. For a fixed centrality (ϵ_i), Δ is minimum for $\Upsilon(1S)$ and increases for the excited states due to the hierarchy in ϵ_s 's. For a fixed Δ , τ_s becomes larger due to the presence of dissipative forces, compared to ideal fluid. In fact, the shear viscosity slows down the expansion at the early stages of the expansion and thus affect the screening of the $\Upsilon(1S)$ most whereas the bulk viscosity slows down the late stages of the expansion and hence the excited states are affected much. This is due to the fact that the shear viscosity is developed at the early stages and diminishes gradually whereas the bulk viscosity sets in late in the proximity of the critical temperature. Thus both the bulk and shear viscosities act as an additional handle to decipher the suppression pattern.

With this understanding, we now analyze the results on the screening energy density contours for the $\Upsilon(1S)$ and $\Upsilon(2S)$ states in Fig.3 at LHC energy, i.e. how the topology of the contour depends on the quarkonium properties, the expansion dynamics etc. The main observations are: i) the size of the contour increases while going from the ground state to the excited states because the screening energy density decreases from $\Upsilon(1S)$ to $\Upsilon(2S)$ states rapidly, so the system takes longer to reach ϵ_s for the excited states, ii) the contour also increases with the increase of the viscous forces because the viscous forces slows down the entire evolution. More specifically the contour of the ground states are affected by the shear term only, whereas the excited states are affected by

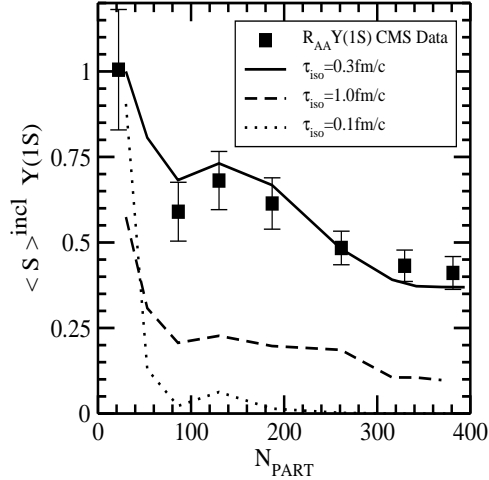


Figure 8: Centrality dependence of the sequential suppression of $\Upsilon(1S)$ for different isotropization times

both. The above observations can be encrypted in the boundary of the screening region (r_s). To understand both the centrality (N_{part}) and transverse momentum (p_T) spectrum of the suppression pattern, we have calculated r_s as a function of the number of participants (N_{part}) for various p_T 's in Fig. 4. It is found that the size of the screening boundary (r_s) increases rapidly with the centrality and explains why there is more suppression in most central collision and less suppression in peripheral collision. To be more specific, for 1S state, the screening boundary initially enlarges rapidly and gets saturated for $N_{\text{part}} \geq 300$, while for the excited states it increases monotonically, with the centrality. This explains why there is a saturation trend in the CMS results for the $\Upsilon(1S)$ suppression for $N_{\text{part}} > 300$ (left panel of Fig. 5) and there is gradual suppression for the excited (2S and 3S) states (Fig. 6). We also notice that for a given centrality, the screening boundary for the $\Upsilon(1S)$ state gets squeezed rapidly for $Q\bar{Q}$ pairs having larger p_T , while the boundary gets swelled for pairs with smaller momenta. Thus for smaller number of participants, the p_T above which a pair can escape, is larger than the larger number of participants. Since the production of partons with smaller p_T 's are more abundant in smaller centralities than the higher centralities, so the above observation explains why there is more suppression even in the smaller centralities (left panel of Fig. 5). However, the sensitivity of the transverse momenta is less prominent for the excited states (right panel of Fig. 4). That is why there is no strong centrality dependence in the suppression pattern for $\Upsilon(2S)$ and $(3S)$ states (Fig 6), in contrast to the $\Upsilon(1S)$ state.

With these ingredients, we explain our results on the inclusive survival probability for the $\Upsilon(1S)$ state computed from the feed down of the excited states (left panel of Fig. 5). We found

that the suppression increases with the centrality upto $N_{\text{part}}=300$ and nearly saturates beyond $N_{\text{part}} > 350$. This finding is compatible with our earlier observation (left panel of Fig. 4), where the screening radius (r_s) is almost independent of the centrality beyond a certain value. We also notice that the inclusive (survival) probability (averaged over the centralities) for $\Upsilon(1S)$ state increases linearly with p_T (right panel of Fig. 5). This is again compatible with our earlier observation, where for a given centrality, r_s increases almost linearly with p_T .

We have also calculated the inclusive survival probability for the $\Upsilon(2S)$ and $(3S)$ states (Fig. 6), which are found to decrease slowly with the centrality. This finding resonates with the earlier observation (right panel of Fig. 4), where for a given p_T , the screening radius (r_s) increases linearly with the centrality and for a given centrality, the p_T dependence of r_s is very slow.

The initial state effects affect the $\Upsilon(nS)$ states in a similar manner, so the possible acceptance and/or efficiency differences cancel out in the ratio, $\Upsilon(nS)/\Upsilon(1S)_{PbPb}$ (with respect to the p - p collisions). Moreover the final state nuclear absorption effects are expected to minimum at LHC energies [71], so we have calculated the double ratio (Fig. 7) at the LHC energy, which shows poor suppression of 2S state with respect to 1S state for peripheral collision and no characteristic dependence on the collision centrality for $N_{\text{part}} > 100$. But CMS results show more suppression of $\Upsilon(2S)$ for peripheral collisions and other approaches [72, 73, 74] also agrees with this fact. This indicate that either their may be some additional suppression mechanisms which are still missing in the theoretical calculations or CMS measurements are not sufficient to disentangle the nuclear effects from medium effects and it could be better resolved on availability of more data from heavy-ion and proton-nucleus collision runs at LHC in future. The results of double ratio shows excited states are suppressed more with respect to ground state.

To explore the effects of the viscous forces on the suppression, we take the shear viscosity to entropy ratio, η/s as 0.08 and 0.3 along with the parametrization of the bulk viscosity, ζ/s from (64). We notice that the suppression increases with the increase of shear viscosity which, in turn, enhances the screening time. Our estimate agrees with the CMS data when the ratio η/s is taken from its perturbative estimate. This seems justified because the screening energy density for the $\Upsilon(1S)$ state is very high where the perturbative calculation seems meaningful. So the $\Upsilon(1S)$ production can be used to constrain the η/s ratio.

Since the physics of isotropization is yet to understand theoretically, so the duration of the pre-equilibrium era is uncertain. Therefore we take the privilege to constrain the arbitrariness of

τ_{iso} by the suppression of bottomonium production (Fig. 8) because Υ (1S) is formed earlier than the isotropization time, which is not the case for Υ (2S) state. We have found that $\tau_{iso}=0.3$ fm looks more plausible as far as CMS data is concerned.

4 Conclusions

In conclusion we have studied the sequential suppression for Υ (1S) and Υ (2S) states at the LHC energy in a longitudinally expanding partonic system, which underwent through the successive pre-equilibrium and equilibrium phases in the presence of dissipative forces. Quarkonium suppression in nucleus-nucleus collisions compared to p - p collisions couples the in-medium properties of the quarkonium states with the dynamics of the expanding medium. In this work we obtained the dissociation temperatures of the quarkonium states by correcting both the perturbative and nonperturbative terms in $Q\bar{Q}$ potential in (an)isotropic medium through the HTL resummed perturbation. We then modeled the pre-equilibrium evolution as anisotropic fluid via the time dependent anisotropic parameter, $\xi(\tau)$ and hard momentum scale, $P_{hard}(\tau)$ while the equilibrium era is governed by the second-order dissipative hydrodynamics in (1+1) Bjorken boost-invariant model and coupled them together to estimate the sequential suppression. The expansion in equilibrium hydrodynamics is controlled by the speed of sound c_s^2 , which could be further handled by the lattice QCD equation of state, the shear (η) and bulk (ζ) viscous forces etc.

The bulk viscosity in conjunction with the shear viscosity enhances the cooling rate and thus causes more suppression to the ground state, however, the bulk viscosity ζ/s is significant for excited states. The sequential suppression is a very complex phenomenon depends on several parameters such as the scale of the dissociation of quarkonium states, the decay of the excited states, the centrality of collision, the transverse momentum, the screening time, the formation time, the dissipative forces etc., including the isotropization time and too early or too late isotropization results in over suppression. The tiny formation time (compared to the isotropization time) and tightly bound character of the bottomonium states help the the suppression of bottomonium to constrain both the isotropization time (0.3 fm) as well as the shear viscosity-to-the entropy ratio (0.3)

Acknowledgments: One of us (BKP) is thankful for some financial assistance from CSIR project (CSR-656-PHY), Government of India. USK is also thankful to Government of Maharashtra for

the financial assistance.

References

- [1] T. Matsui and H. Satz, Phys. Lett. B **178**, 416 (1986).
- [2] N. Brambilla, J. Alghieri, A. Vairo and P. Petreczky, Phys. Rev. D **78**, 014017 (2008).
- [3] A. Beraudo, J. P. Blaizot, and C. Ratti, Nucl. Phys. A **806**, 312 (2008).
- [4] M. Laine, O. Philipsen, and M. Tassler, JHEP. **09**, 066 (2007).
- [5] K. G. Wilson. Phys. Rev. (1974). K. G. Wilson. Phys. Rev. (1974).
- [6] Y. Makeenko, Physics of Atomic Nuclei **73** 5,878(2010).
- [7] J. Berges, Sz. Borsnyi, D. Sexty, and I.-O. Stamatescu Phys. Rev. D **75**, 045007(2007).
- [8] A. Barchielli, E. Montaldi and G. M. Prospero Nucl. Phys. B **296**, 625 (1988).
- [9] A. Rothkopf Mod. Phys. Lett. A **28**, 1330005 (2013).
- [10] M. Laine, O. Philipsen, P. Romatschke, and M. Tassler, JHEP **03** 054 (2007).
- [11] F. Karsch, M. G. Mustafa, M. H. Thoma, Phys. Lett. B **497**, 249 (2001).
- [12] A. Mocsy and P. Petreczky, Eur. Phys. J. C **43**, 77 (2005); A. Mocsy and P. Petreczky, Phys. Rev. D **73**, 074007 (2006); A. Mocsy and P. Petreczky, Phys. Rev. Lett. **99**, 211602 (2007); A. Mocsy and P. Petreczky, Phys. Rev. D **77**, 014501 (2008).
- [13] C. Y. Wong, Phys. Rev. C **72**, 034906 (2005).
- [14] D. Cabrera and R. Rapp, Phys. Rev. D **76**, 114506 (2007).
- [15] W. M. Alberico, A. Beraudo, A. De Pace, A. Molinari, Phys. Rev. D **77**, 017502 (2008).
- [16] Ph. de Forcrand, et.al Phys. Rev. D **63**, 054501 (2001).
- [17] B. Schenke and M. Strickland, Phys. Rev. D **76**, 025023 (2007).

- [18] M. Martinez and M. Strickland, Phys. Rev. Lett. **100**, 102301 (2008); M. Martinez and M. Strickland, Phys.Rev. C **78**, 034917 (2008).
- [19] R. Vogt, Phys. Rev. C **81**, 044903 (2010).
- [20] R. Vogt, Phys. Rev. C **61**, 035203 (2000); [arXiv:hep-ph/9907317].
- [21] S. Gavin and J. Milana, Phys. Rev. Lett. **68**, (1992) 1834.
- [22] X. M. Xu, D. Kharzeev, H. Satz and X. N. Wang, Phys. Rev. C **53**,3051 (1997).
- [23] B. K. Patra and V. J. Menon, Euro. Phys. J. C **37**, 115 (2004); B. K. Patra and V. J. Menon, Euro. Phys. J. C **44**, 567 (2005); B. K. Patra and V. J. Menon, Euro. Phys. J. C **48**, 207 (2006).
- [24] R. Vogt, Phys. Rep. **310**,197 (1999).
- [25] F. Karsch, M. T. Mehr, H. Satz, Z. Phys. C **37**, 617 (1988).; F. Karsch, H. Satz, Z. Phys.C **51**, 209 (1991).
- [26] M. Martinez and M. Strickland, Nucl. Phys. A **856**, 68 (2011); M. Martinez and M. Strickland, Nucl. Phys. A**848**, 183 (2010); M. Martinez, R. Ryblewski, and M. Strickland, Phys. Rev. C **85**,064913 (2012).
- [27] R. Ryblewski, and W. Florkowski, J. Phys. G **38**, 015104 (2011);R. Ryblewski, and W. Florkowski Euro. Phys. J. C **71**, 1761 (2011)
- [28] R. Ryblewski, W. Florkowski, Phys. Rev. C **85**, 064901 (2012);W. Florkowski, R. Ryblewski, and M. Strickland, Phys. Rev. D **86**, 085023 (2012).
- [29] W. Florkowski and R. Ryblewski, Phys. Rev. C **83**, 034907(2011); arXiv:1007.0130.
- [30] A. Dumitru, Y. Guo and M. Strickland, Phys. Lett. B **662**, 37 (2008); A. Dumitru, Y. Guo and M. Strickland, Phys. Rev. D **79**, 114003 (2009);A. Dumitru, Y. Guo, A. Mocsy and M. Strickland, Phys. Rev. D **79**, 54019 (2009).
- [31] Y. Burnier, M. Laine and M. Vepsalainen, arXiv:0903.3467.
- [32] V. Agotiya, V. Chandra and B. K. Patra, Phys. Rev. C **80**, 025210 (2009).

- [33] Lata Thakur, U. Kakade and B. K. Patra, Phys. Rev. D (In press), arXiv:1401:0172.
- [34] Lata Thakur, N. Haque, U. Kakade and B. K. Patra Phys.Rev. D **88** , 054022 (2013).
- [35] M. E. Carrington, H. Defu, and M. H. Thoma, Eur. Phys. J.C **7**, 347 (1999); Phys. Rev. D **58**, 085025 (1998).
- [36] S. Chatrchyan *et al.*, Phys. Rev. Lett. **109**, 222301 (2012).
- [37] P. Arnold, J. Ienghan, G. Moore and L. Yaffe, Phys. Rev. Lett.**94**, 072302 (2005).
- [38] U. Romatschke, Phys. Rev. Lett. **99**, 172301 (2007).
- [39] A. Rebhan, P. Romatschke and M. Strickland, Phys. Rev. Lett.**94**, 102303 (2005).
- [40] M. Laine, O. Philipsen, M. Tassler, and P. Romatschke, JHEP **0703**, 054 (2007).
- [41] M. Laine, Nucl. Phys. A **820**, 25 C (2009).
- [42] M. Strickland, Phys. Rev. Lett. **107**, 132301 (2011), arXiv:1106.2571.
- [43] M. Strickland and D. Bazow, Nucl. Phys. A **879**, 25 (2012).
- [44] E. Megias, E. Ruiz Arriola and L. L. Salcedo, Indian J.Phys. **85** 1191 (2011).
- [45] E. Megias, E. Ruiz Arriola and L. L. Salcedo, Phys. Rev. D **75**, 105019 (2007).
- [46] Y. Burnier, M. Laine, and M. Vepsalainen, JHEP. **01**, 043 (2008).
- [47] M. Margotta, K. McCarty, C. McGahan, M. Strickland and D. Yager-Elorriaga, Phys. Rev. D **83**, 105019 (2011); P. Romatschke and M. Strickland, Phys. Rev. D **68**,036004 (2003);M. Martinez and M. Strickland Phys. Rev. C **79** 044903 (2009).
- [48] P. Romatschke and M. Strickland, Phys. Rev. D **68**, 036004 (2003).
- [49] S. Mrowczynski, Phys. Lett B **314**, 118 (1999).
- [50] P. Arnold, G. D. Moore and L. G. Yaffe, JHEP **05**, 051 (2003).
- [51] S. Mrowczynski and M. H. Thoma, Phys. Rev. D **62**, 036011 (2000) .
- [52] M. Strickland, J. Phys. G: Nucl. Part. Phys. **34**, S429 (2007).

- [53] M. Martinez and M. Strickland, Phys. Rev. C **78** 034917 (2008).
- [54] S. Borsanyi, G. Endrodi, Z. Fodor, S.D. Katz, S.Krieg, C. Ratti, and K. Szabo, arXiv:1204.6710v2; JHEP **11**, 077 (2011).
- [55] W. Israel and J. M. Stewart, Annals Phys. **118**, 341 (1979).
- [56] U. W Heinz, arXiv:nucl-th/0512049.
- [57] A. Muronga, Phys. Rev. C **69**, 034903 (2004).
- [58] R. Baier, P. Romatschke, and U. A. Wiedemann, Phys. Rev. C **73**, 064903 (2006).
- [59] R. Baier, P. Romatschke, D. Son, A. Starinets, and M. Stephanov, JHEP **04**, 100 (2008).
- [60] R. Fries, B. Muller and A. Schafer, Phys. Rev. C **78**, 034913 (2003).
- [61] P. Arnold, G. D. Moore, L. G. Yaffe, JHEP **11**, 001 (2000).
- [62] P. Kovtun, D. Son and A. Starinets, Phys. Rev. Lett. **94**, 111601 (2005).
- [63] A. Jaiswal, R. Bhalerao and S. Pal, Phys. Rev. C **87**, 021901(2013).
- [64] K. Rajagopal and N. Tripuraneni, JHEP **1003**, 018 (2010).
- [65] H. B. Mayer, Phys. Rev. Lett. **100**, 162001 (2008).
- [66] M. Prakash, M. Prakash, R. Venugopalan and G. Welke, Phys. Rept. **227**, 321 (1993).
- [67] T. Affolder et al., Phys. Rev. Lett. **84**, 2094 (2000).
- [68] Phenix Collaboration, Phys. Rev. C **71**, 034908 (2005);Erratum-ibid.C71:049901,2005.
- [69] CMS Collaboration, CMS-HIN-11-003, Phys. Rev. Lett. **109**, 152303 (2012).
- [70] T. Hirano, Phys. Rev. C **65** 011901(R) (2001).
- [71] Z. W. Lin and C. M. Ko, Phys. Lett. B **503**, 104 (2001).
- [72] T. Song, K. C.Ha, and C. M.Ko, Phys. Rev. C **85**, 014902 (2012).
- [73] A. Emerick, X Zhao and R. Rapp, Eur. Phys. J. A **48**, 72 (2012).
- [74] Felix Nendzig and G. Wolschin, arXiv:1210.8366v2[hep-ph].